Ann. Geophys., 29, 2287–2304, 2011
www.ann-geophys.net/29/2287/2011/
doi:10.5194/angeo-29-2287-2011

Annales Geophysicae

Interhemispheric comparison of GPS phase scintillation at high latitudes during the magnetic-cloud-induced geomagnetic storm of 5–7 April 2010

P. Prikryl[1], L. Spogli[2], P. T. Jayachandran[3], J. Kinrade[4], C. N. Mitchell[4], B. Ning[5], G. Li[5], P. J. Cilliers[6], M. Terkildsen[7], D. W. Danskin[8], E. Spanswick[9], E. Donovan[9], A. T. Weatherwax[10], W. A. Bristow[11], L. Alfonsi[2], G. De Franceschi[2], V. Romano[2], C. M. Ngwira[6], and B. D. L. Opperman[6]

[1]Communications Research Centre Canada, Ottawa, ON, Canada
[2]Istituto Nazionale di Geofisica e Vulcanologia, Rome, Italy
[3]Physics Department, University of New Brunswick, Fredericton, NB, Canada
[4]Department of Electronic and Electrical Engineering, University of Bath, Bath, UK
[5]Institute of Geology and Geophysics, Chinese Academy of Sciences, Beijing, China
[6]South African National Space Agency, Hermanus, South Africa
[7]IPS Radio and Space Services, Bureau of Meteorology, Haymarket, NSW, Australia
[8]Geomagnetic Laboratory, Natural Resources Canada, ON, Canada
[9]Department of Physics and Astronomy, University of Calgary, AB, Canada
[10]Department of Physics and Astronomy, Siena College, Loudonville, NY, USA
[11]Geophysical Institute, University of Alaska Fairbanks, Fairbanks, AK, USA

Received: 1 September 2011 – Revised: 2 December 2011 – Accepted: 9 December 2011 – Published: 21 December 2011

Abstract. Arrays of GPS Ionospheric Scintillation and TEC Monitors (GISTMs) are used in a comparative scintillation study focusing on quasi-conjugate pairs of GPS receivers in the Arctic and Antarctic. Intense GPS phase scintillation and rapid variations in ionospheric total electron content (TEC) that can result in cycle slips were observed at high latitudes with dual-frequency GPS receivers during the first significant geomagnetic storm of solar cycle 24 on 5–7 April 2010. The impact of a bipolar magnetic cloud of north-south (NS) type embedded in high speed solar wind from a coronal hole caused a geomagnetic storm with maximum 3-hourly Kp = 8- and hourly ring current Dst = −73 nT. The interhemispheric comparison of phase scintillation reveals similarities but also asymmetries of the ionospheric response in the northern and southern auroral zones, cusps and polar caps. In the nightside auroral oval and in the cusp/cleft sectors the phase scintillation was observed in both hemispheres at about the same times and was correlated with geomagnetic activity. The scintillation level was very similar in approximately conjugate locations in Qiqiktarjuaq (75.4° N; 23.4° E CGM lat. and lon.) and South Pole (74.1° S; 18.9° E), in Longyearbyen (75.3° N; 111.2° E) and Zhongshan (74.7° S; 96.7° E), while it was significantly higher in Cambridge Bay (77.0° N; 310.1° E) than at Mario Zucchelli (80.0° S; 307.7° E). In the polar cap, when the interplanetary magnetic field (IMF) was strongly northward, the ionization due to energetic particle precipitation was a likely cause of scintillation that was stronger at Concordia (88.8° S; 54.4° E) in the dark ionosphere than in the sunlit ionosphere over Eureka (88.1° N; 333.4° E), due to a difference in ionospheric conductivity. When the IMF tilted southward, weak or no significant scintillation was detected in the northern polar cap, while in the southern polar cap rapidly varying TEC and strong phase scintillation persisted for many hours. This interhemispheric asymmetry is explained by the difference in the location of solar terminator relative to the cusps in the Northern and Southern Hemisphere. Solar terminator was in the immediate proximity of the cusp in the Southern Hemisphere where sunlit ionospheric plasma was readily convected into the central polar cap and a long series of patches was observed. In contrast, solar terminator was far poleward of the northern cusp thus reducing the entry of sunlit plasma and formation of dense patches. This is consistent with the observed and modeled seasonal variation in occurrence of polar cap patches. The GPS scintillation and TEC data analysis is supported by data from ground-based networks of magnetometers, riometers, ionosondes, HF radars and all-sky imagers, as well as particle flux measurements by DMSP satellites.

Correspondence to: P. Prikryl
(paul.prikryl@crc.gc.ca)

Published by Copernicus Publications on behalf of the European Geosciences Union.

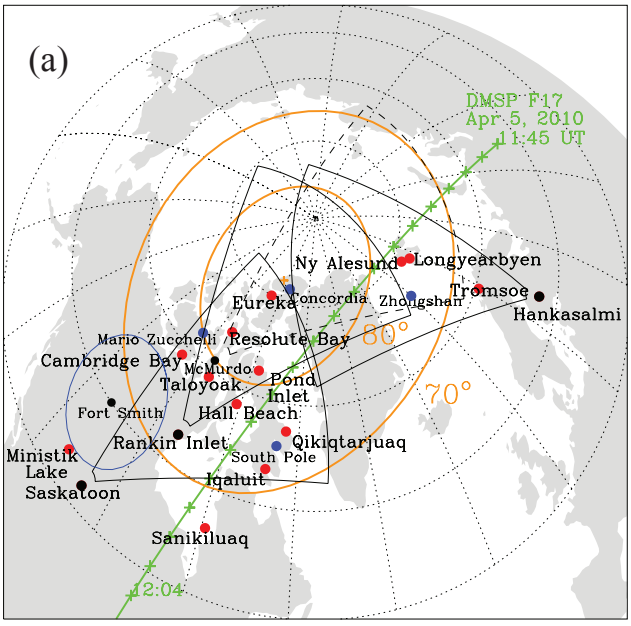

Fig. 1a. The CHAIN and European GISTM arrays (red dots) and fields of view of SuperDARN radars in Saskatoon, Rankin Inlet and Hankasalmi. Conjugate locations of four Antarctic GPS receivers (blue dots) and the field of view of the McMurdo SuperDARN radar (dashed line) are superposed. The location and field of view of an all-sky imager in Fort Smith is shown. Corrected geomagnetic (CGM) latitudes 70° N and 80° N and DMSP F17 satellite track are superposed.

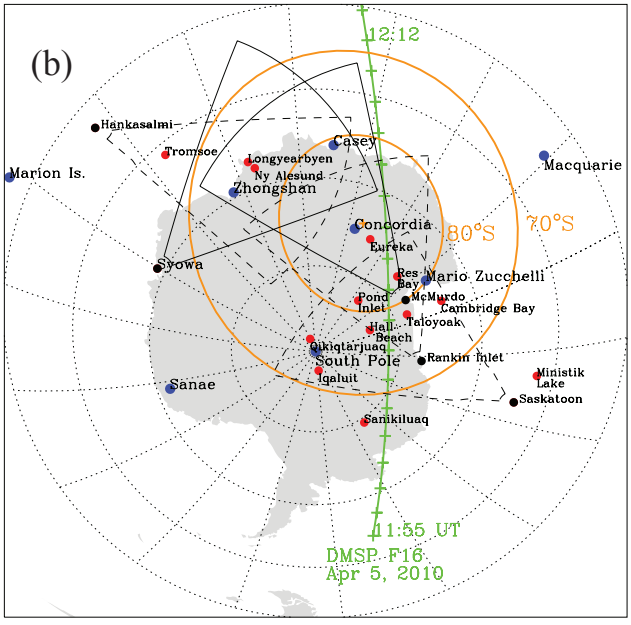

Fig. 1b. GPS scintillation receivers in Antarctica (blue dots) and the field of view of the SuperDARN radar in McMurdo and Syowa East. Conjugate locations of northern GISTM arrays (red dots) and fields of view of Saskatoon, Rankin Inlet and Hankasalmi SuperDARN radar (dashed line) are superposed. Radar locations are shown by black dots. Corrected geomagnetic (CGM) latitudes 70° S and 80° S and DMSP F16 satellite track are superposed.

Keywords. Ionosphere (Ionospheric irregularities) – Magnetospheric physics (Storms and substorms) – Radio science (Space and satellite communication)

1 Introduction

Magnetic clouds (MCs) are a subset of interplanetary coronal mass ejections (ICMEs) showing a strong and smoothly rotating magnetic field, a low proton temperature, and a ratio of the plasma pressure to the magnetic pressure (plasma β) significantly lower than unity (Burlaga et al., 1981). Huttunen et al. (2005) divided MCs into "bipolar" and "unipolar" based on the axial orientation of the magnetic field and studied geoeffectiveness of MCs during various phases of the solar cycle. They found that near the solar minimum and in the rising phase of solar activity most MCs are bipolar. Echer et al. (2005) found that 77 % of MCs are followed by intense or moderate geomagnetic storms (Dst < -50 nT). The geoeffectiveness of MCs and ICMEs in general largely depends on the polarity of the IMF B_Z, the magnetic field strength (B) and their products with solar wind speed (VB and VB_Z) (Kumar and Raizada, 2010; Richardson and Cane, 2011). Regarding the interplanetary causes of geomagnetic storms, Kumar et al. (2005) reported that about 30 % of magnetic storms were associated with MCs. The ionospheric effects included VHF scintillation in the post-midnight period around the time of maximum storm ring current. High pressure pulses on the leading and trailing edges of MCs also result in magnetospheric disturbances including compression and deformation, large scale motions of the magnetic tail and initiations of substorms and storms (Yermolaev et al., 2000).

The extended periods of northward or southward interplanetary IMF during an MC passage can produce dynamic and intense polar precipitation and auroras or polar cap patches of ionization, respectively, as shown for the MC event of 10 January 1997 (Elsen et al., 1998; Steele et al., 1998). For the same event, Ho et al. (1998) generated global ionospheric TEC maps that showed significant differences in distribution and variations of TEC between the Northern and Southern Hemispheres. In particular, their Fig. 2 shows a dense tongue of ionization (TOI) traversing the southern polar cap while at the same time a TOI appears to have been absent in the northern polar cap where only weaker patches were observed optically (Steele et al., 1998) and with an ionosonde in Eureka. Under disturbed and dynamic conditions TOI can be fragmented into smaller structures including scintillation-causing ionospheric irregularities (see, e.g. Mitchell et al., 2005). The dynamics of such irregularities

Table 1. Geographic and corrected geomagnetic coordinates of GISTM sites.

Station	Geographic latitude	Geographic longitude	CGM latitude	CGM longitude
Northern Hemisphere	(° N)	(° E)	(° N)	(° E)
Ny Ålesund (NYA)	78.92	11.92	76.24	110.19
Longyearbyen (LYB)	78.17	15.99	75.26	111.22
Tromsø (TRO)	69.58	19.22	66.59	102.70
Eureka (EUR)	79.99	274.10	88.08	333.43
Resolute Bay (RES)	74.75	265.00	83.06	321.24
Pond Inlet (PON)	72.69	282.04	81.49	1.78
Cambridge Bay (CAM)	69.12	254.97	77.03	310.12
Taloyoak (TAL)	69.54	266.44	78.59	330.10
Hall Beach (HAL)	68.78	278.74	78.12	354.22
Qikiqtarjuaq (QIK)	67.53	295.97	75.38	23.37
Iqaluit (IQA)	63.73	291.46	72.41	14.77
Sanikiluaq (SAN)	56.54	280.77	66.66	356.90
Ministik Lake (MST)	53.35	247.03	60.70	307.36
Southern Hemisphere	(° S)	(° E)	(° S)	(° E)
Concordia (DMC)	75.10	123.33	88.75	54.36
Mario Zucchelli (BTN)	74.70	164.11	79.97	307.69
South Pole (SPO)	90.00	0.00	74.10	18.91
Zhongshan (ZSH)	69.37	76.38	74.68	96.73
Sanae (SNA)	71.67	357.16	61.42	43.78
Marion Island (MAR)	46.88	37.86	51.91	93.10
Macquarie Island (MQI)	54.50	158.95	64.37	248.32

is controlled by the IMF as shown, for example during the October and November 2003 storms (De Franceschi et al., 2008).

Ionospheric irregularities embedded in polar patches that are produced in the cusp and also the auroral irregularities produced by intense auroras, result in rapid fluctuations of radio wave amplitude and phase, called scintillation. Scintillation may affect performance and operational capabilities of radio communication and navigation systems using satellite-to-ground links near the magnetic equator and at high latitudes. The present paper focuses on the high-latitude ionospheric effects including GPS phase scintillation, rapid variations in TEC, and cycle slips. The scintillation and TEC variations were caused by an impact of an MC that was immersed in high speed solar wind and produced strong but sometimes asymmetric response in the northern and southern high latitudes on 5–7 April 2010.

2 Instruments and techniques

The GPS Ionospheric Scintillation and TEC Monitors (GISTMs) are operated in northern Europe and Antarctica (De Franceschi et al., 2006; Li et al., 2010; Ngwira et al., 2010). The Canadian High-Arctic Ionospheric Network (CHAIN) is an array of GISTM receivers and ionosondes (Jayachandran et al., 2009) to study the high-latitude ionosphere in the North-American sector. Figure 1a shows the CHAIN and European GISTM arrays, fields of view of SuperDARN radars and "conjugate" locations of some Antarctic GPS receivers (blue dots) shown at northern magnetic latitudes. Figure 1b shows locations of GPS receivers, fields of view of SuperDARN radars and "conjugate" locations of Arctic GPS receivers (red dots) shown at southern magnetic latitudes. Table 1 lists the geographic and corrected geomagnetic coordinates of GISTMs used in this paper.

A GISTM of the GSV 4004B series consists of a NovAtel OEM4 dual frequency receiver with special firmware specifically configured to measure and log high rate (50 Hz) power and phase of the GPS L1 signal. The receiver provides ionospheric TEC from the GPS L1 and L2 signals. It can also automatically compute and log the amplitude scintillation index, S_4, which is the standard deviation of the received power normalized by its mean value, and the phase scintillation index σ_Φ, the standard deviation of the detrended phase using a filter in the receiver with 0.1 Hz cutoff. A minimal elevation of 20° is used to reduce the impact of non-scintillation related tracking errors such as multipath. Only phase scintillation index σ_Φ is used in this study. The S_4 index is not considered since it was generally very low even when σ_Φ was enhanced, as is usually the case at high latitudes (Kintner et al., 2007). Large ionospheric plasma drifts at high

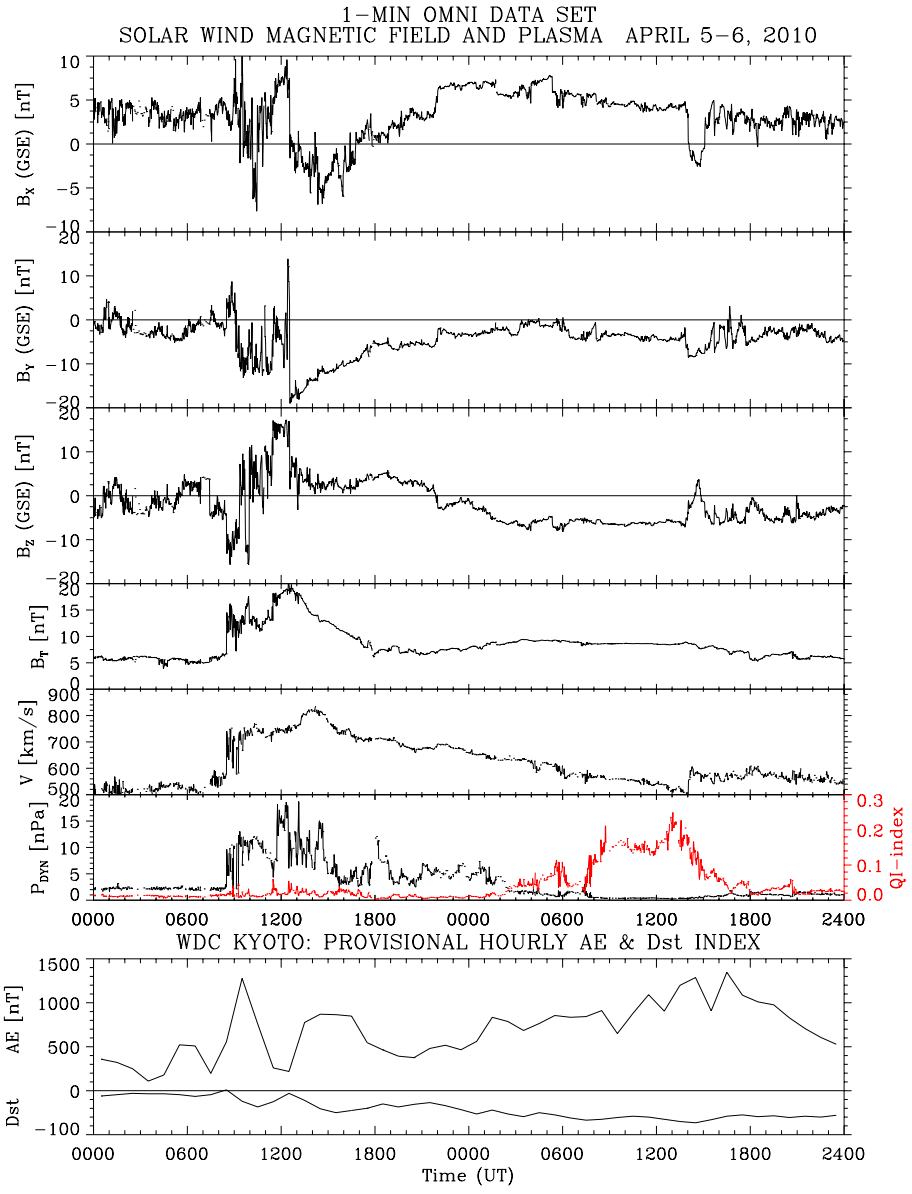

Fig. 2. Solar wind magnetic field and plasma parameters from OMNIWeb data set combining available solar wind monitor data projected to the nose of the Earth's bow shock. Quasi invariant index is superposed in red line. Provisional hourly values of AE and Dst indices are shown in the bottom panel.

latitudes cause the GPS receivers to record negligible amplitude scintillation index S_4, while phase scintillation is much enhanced. For amplitude scintillation, the Fresnel frequency $f_F = v/(2\lambda z)^{0.5}$, where v is the ionospheric drift, λ is the wavelength of GPS L1 frequency, z is the mean ionospheric height. When v is large, the Fresnel frequency is moved to a range beyond the Nyquist frequency, so that amplitude scintillation is not detected by the receiver. On the other hand, the phase scintillation index is controlled by the power spectral density of irregularities at 0.1 Hz, the low cut-off frequency of the receiver. At high convection velocity v, the irregularity scale length at the cut-off frequency will be large and will correspond to a large power spectral density causing a large value of the phase scintillation index.

A tomographic technique known as ionospheric imaging is used to construct TEC maps. The method is an adaptation of the MIDAS (Multi-Instrument Data Assimilation System) method developed by Spencer and Mitchell (2007) and the IDA4D (Ionospheric Data Assimilation Four-Dimensional) technique by Bust et al. (2004). The ionospheric electron density was reconstructed on a three-dimensional grid of resolution 4° in latitude, 4° in longitude and 40 km in altitude

(Kinrade et al., 2011). Electron density images were produced with 10-min GPS data samples using a tomographic space-time inversion. The inversion required regularization, which sought to minimize the rate of change of electron density gradients in space and time.

The GISTM arrays are supported by radars, optical instruments and magnetometers of the Canadian Geospace Monitoring (CGSM) program (Liu, 2005), the Istituto Nazionale di Geofisica e Vulcanologia (INGV) magnetometers in Antarctica, the IMAGE array (Viljanen and Häkkinen, 1997) and magnetometer data provided by INTERMAGNET (www.intermagnet.org). The Northern Solar Terrestrial Array (NORSTAR) (Donovan et al., 2003) is an optical and radio facility designed to remotely sense auroral precipitation on a continental scale. NORSTAR consists of CCD-based All-Sky Imagers (ASIs), Meridian Scanning Photometers (MSPs), and riometers. Particle data obtained during high-latitude overpasses by Defense Meteorological Satellite Program (DMSP) satellites (http://sd-www.jhuapl.edu/Aurora/) are used to support the scintillation study.

The Super Dual Auroral Radar Network (SuperDARN) is a network of coherent-backscatter HF radars with fields of view covering a large fraction of the northern and southern high-latitude ionosphere (Greenwald et al., 1995; Chisham et al., 2007). The radars transmit at frequencies 8–20 MHz along 16 successive continuously swept azimuthal beams. The range bins are 45 km long in standard operations (75 range gates) and the dwell time for each beam is 7 s. A full 16-beam scan with successive beams separated by 3.24° covers about 52° in azimuth every 2 min. Line-of-sight (LOS) Doppler velocity, spectral width and backscatter power from field-aligned ionospheric (FAI) plasma irregularities are routinely measured.

3 High speed solar wind on 5–6 April 2010

The interplanetary propagation of the fast ICME event that included a geoeffective MC was discussed in some detail by Möstl et al. (2010). The ICME/MC was embedded in a high speed plasma stream from a coronal hole with solar wind speed V reaching up to 820 km s^{-1} (Fig. 2). As typically the case (Richardson and Zhang, 2008), an upstream shock and a sheath of compressed solar wind bounded the leading edge of the ICME/MC. Dynamic pressure pulses of up to 18 nPa and a strong southward IMF B_Z in the sheath sparked intense substorm activity that was followed by the strongest geomagnetic storm of the year (maximum Kp index of 8- and Dst index reaching −73 nT). The upstream shock was associated with a steep southward turning of the IMF, followed by an oscillation of B_Z between large negative and large positive values before turning northward and later rotating more gradually from northward to southward inside of the north-south (NS) type cloud. In the cloud interior, the proton temperature and plasma beta were low, less than 10^5 K and 0.2, respectively. The magnetic-field magnitude B peaked at 20 nT at the beginning of the cloud but dropped to about 7 to 9 nT, which was still exceeding the average value of about 5 nT before and after the event. Figure 2 shows intense and dynamic (ram) pressure P_{DYN} pulses at the leading edge of the cloud followed by a period of enhanced QI index (red line) in the cloud interior. The quasi-invariant index (Osherovich et al., 1999) is defined as $\mathrm{QI} \equiv (B^2/2\mu_0)/(\rho V^2/2) = M_{\mathrm{A}}^{-2}$, where μ_0 is permeability of free space, ρ is plasma density, V is plasma velocity, and M_{A} is the magnetic Mach number ($M_{\mathrm{A}} = V/V_{\mathrm{A}}$, where V_{A} is the Alfvén speed). As a single non-dimensional quantity of fundamental importance, QI characterizes the solar wind geoeffectiveness and correlates with solar activity indices. The index is equivalent to the ratio of the solar-wind magnetic to ram pressures, or the inverse of the magnetic Mach number squared. To characterize the geomagnetic response to the solar wind, the provisional auroral electrojet index AE and the storm ring current Dst index are shown in Fig. 2. The arrival of the upstream shock combined with strong southward IMF caused a substorm as a result of very large dipolarization of the Earth's magnetic field observed at geostationary orbit in the midnight sector (Singer et al., 2010).

4 The high-latitude ionosphere response

4.1 Auroral and cusp activity

On 5 April 2010, an auroral breakup event (∼05:05 UT) that preceded the arrival of the upstream shock (08:30 UT), and the substorm that closely followed it, were captured by all-sky imagers, riometers and magnetometers in northwestern Canada. The auroral 557.7-nm emission brightening and poleward expansion for both events are shown in a keogram constructed from all-sky images obtained from Fort Smith (Fig. 3a). Cosmic noise absorption observed by riometers at 30 MHz is a good proxy for intensity of precipitating energetic electrons and the 557.7-nm emission. Figure 3b shows the riometer absorption and the 557.7-nm emission intensity in the zenith at Fort Smith. The absorption decreased at high latitudes but the poleward expanding aurora reached Cambridge Bay at 05:20 UT and Taloyoak at 06:00 UT. The all-sky imager at Taloyoak (not shown) observed aurora rapidly moving into the field of view from the south, which resulted in a sharp increase in riometer absorption and was closely associated with an onset of phase scintillation as discussed below.

The auroral substorm expansion after 09:00 UT (Fig. 3a) caused much stronger riometer absorption across auroral latitudes but the absorption diminished at high latitudes. The ground magnetic perturbations during the substorm exceeded 1200 nT at most auroral sites in the North American sector, reaching a maximum of about 2400 nT in Dawson, Yukon, at 09:15 UT. Intense phase scintillation was observed following

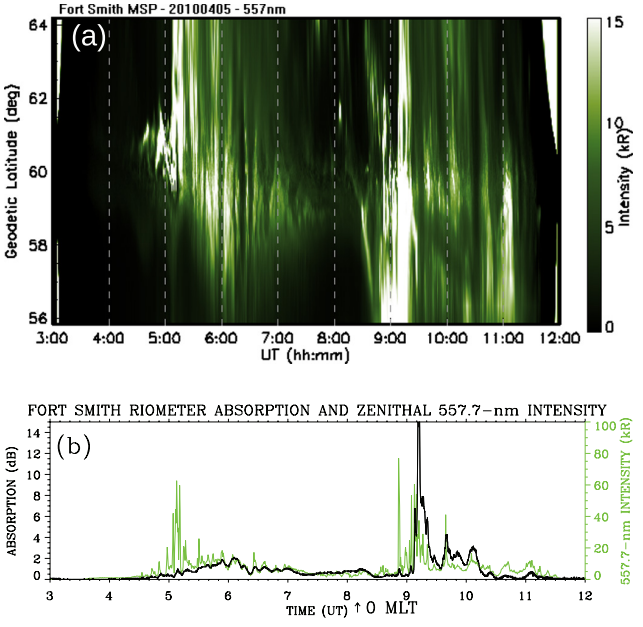

Fig. 3. (a) The 557.7-nm auroral emission as a function of geodetic latitude and UT extracted from all-sky images and **(b)** cosmic noise absorption observed in Fort Smith (60.0° N, 248.1° E). The zenithal 557.7-nm intensity (green line) is superposed. The arrow indicates magnetic local midnight.

the upstream shock at auroral CHAIN stations in Ministik Lake, Sanikiluaq, Iqaluit, Qikitarjuaq, Taloyoak and Cambridge Bay but it was significantly reduced in the polar cap at Pond Inlet, Resolute Bay and Eureka. This is consistent with strong decameter irregularities and enhanced convection observed over the poleward edge of the nightside auroral oval while there was no backscatter detected over the central polar cap (Fig. 4a).

The upstream shock arrival coupled with strong southward IMF (Fig. 2) caused intense ionospheric convection with cross-polar-cap-potential exceeding 100 kV in the Northern Hemisphere. Figure 4 shows the northern and southern SuperDARN convection maps at 08:38 UT. In the Scandinavian sector, scintillation data were available from Ny Ålesund (two receivers at 76.2° N CGM lat.), Longyearbyen (75.3° N) and Tromsø (66.6° N). Longyearbyen along with approximately conjugate Zhongshan station (74.7° S) in Antarctica were located in the cusp. Enhanced convection of up to 2000 m s^{-1} was observed in the northern cusp. The scintillation event started in Longyearbyen and Zhongshan at ∼08:30 UT as a direct response to a pressure pulse that was observed as a sudden impulse (SI) event by magnetometers in Scandinavia. At Tromsø, much weaker scintillation was delayed until 09:00 UT.

Figure 5a shows the rate of TEC change, phase scintillation index σ_Φ, and numerous cycle slips observed in Cambridge Bay. A cycle slip (Horvath and Crozier, 2007) is defined here as a jump in differential phase TEC of more than or equal to 1.5 TECU in one second (1 TEC Unit corresponds to 10^{16} electrons m^{-2}). The GPS satellites are identified by the receiver by means of their pseudo random noise (PRN) codes and satellite numbers, 1–32, are coded by color in Figs. 5–7. The phase scintillation and cycle slips were closely associated with the ground magnetic horizontal field H-component perturbations measured at Cambridge Bay. At Taloyoak, the magnetogram data were not available but the onsets of phase scintillation occurred in conjunction with riometer absorption onsets (Fig. 5b). Phase scintillation intensified again in the pre-noon cusp/cleft sector starting from ∼14:00 UT after intense solar wind dynamic pressure pulses caused ULF wave activity that was observed in Cambridge Bay (Fig. 5a). The pressure pulses were accompanied with large-amplitude oscillations of the IMF that become mostly northward in the compressed interaction region at the leading edge of high-speed solar wind stream (Fig. 2).

South Pole (74.1° S CGM latitude) is approximately conjugate with Qiqiktarjuaq (75.4° N) and Iqaluit (72.9° N). Figure 6a shows that concurrent short bursts of phase scintillation were observed at these sites during auroral events before the MC event at ∼02:30–03:30 and at ∼06:00 UT and, as a response to the upstream shock arrival and substorm onset, at ∼08:35 and 09:20 UT. Continuous phase scintillation persisted through the morning until noon, while at the same time very similar magnetic perturbations (ULF waves) were observed in Iqaluit and South Pole.

Longyearbyen (75.3° N) and Zhongshan (74.7° S) were located in the cusp (Fig. 4) when the upstream shock arrived and strong phase scintillation occurred between 08:30 and 13:00 UT. The observed rate of TEC change and σ_Φ scintillation index in Longyearbyen and Zhongshan were comparable in intensity as shown in Fig. 6b. The convection in the southern cusp may appear to be weaker (Fig. 4b) but this can be attributed to insufficient backscatter. In the evening sector, concurrent scintillation was again observed at these two stations at ∼19:00, 21:00 and 23:00 UT with higher values of σ_Φ in Longyearbyen. In the morning sector prior to the MC event, however, moderate scintillations events in Longyearbyen at 05:00 and 07:00 UT were associated with only low level scintillation in Zhongshan.

In a different longitude sector, Mario Zucchelli station (80.0° S) is approximately conjugate with Cambridge Bay (77.0° N) and Taloyoak (78.6° N). Two top rows in Fig. 7 show the rate of TEC change and σ_Φ scintillation index at Mario Zucchelli on 5 and 6 April. On 5 April, auroral scintillation events starting at ∼06:00 and 08:30 UT and the cusp/cleft scintillation starting at ∼15:00 UT were approximately concurrent with scintillation events observed in Cambridge Bay and Taloyoak (Fig. 5a and b). However, the scintillation at Mario Zucchelli was generally weaker, with σ_Φ rarely exceeding 0.5 radians. The perturbations of the ground magnetic field H component at the conjugate sites also approximately coincided but the first auroral event at ∼06:00 UT, and the morning ULF activity starting after

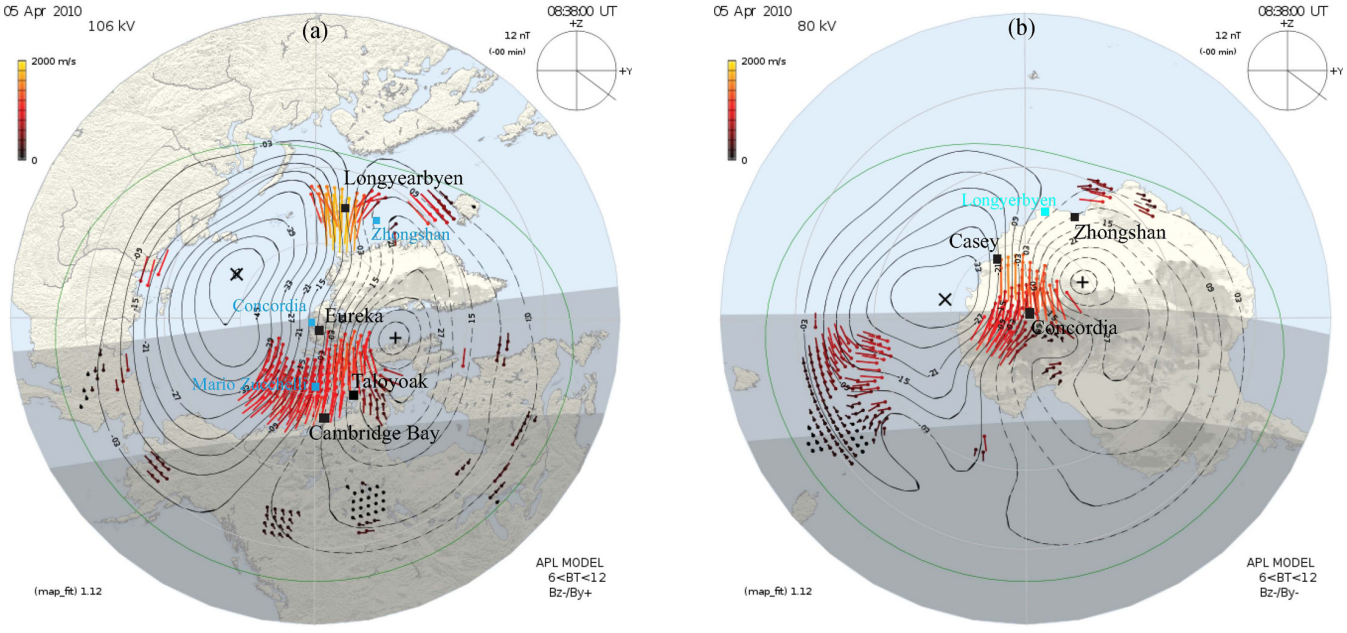

Fig. 4. **(a)** Northern and **(b)** Southern Hemisphere SuperDARN convection and potential maps after the upstream shock arrival. CGM coordinates are used and 12:00 MLT is at the top. Solar terminator at sea level and F-region altitude is shown. F-region in darkness is shaded as darker grey.

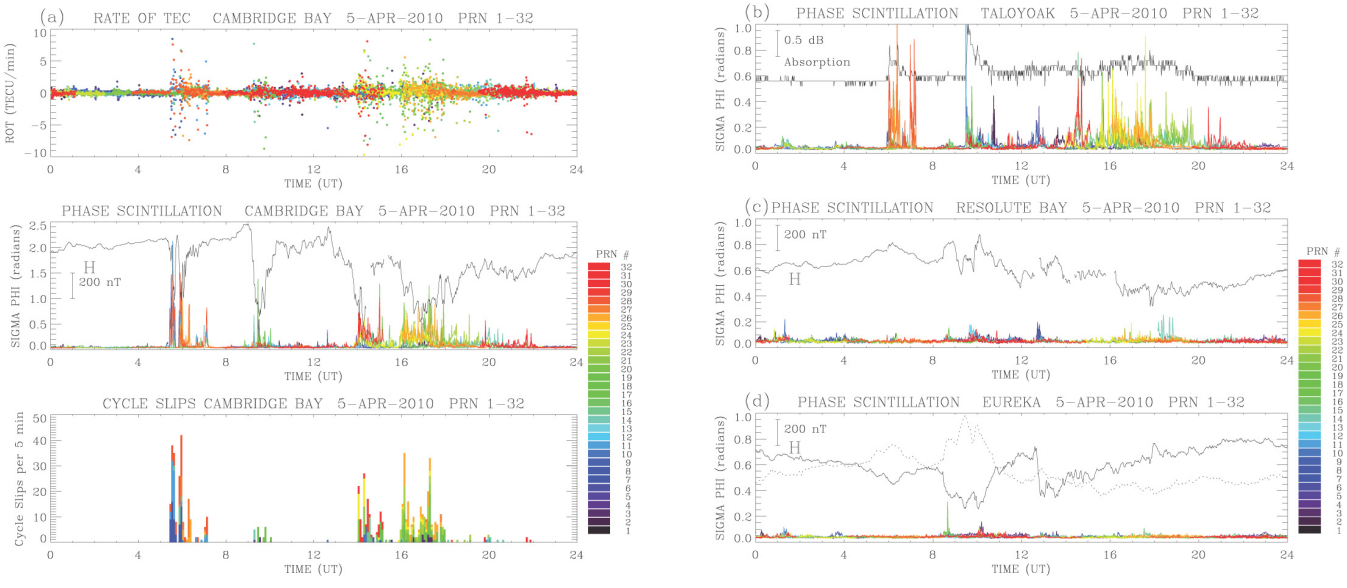

Fig. 5. **(a)** The rate of TEC (ROT) change, phase scintillation index σ_Φ and number of cycle slips in Cambridge Bay observed at elevations above 20° on 5 April 2010. Only phase scintillation index σ_Φ is shown for **(b)** Taloyoak, **(c)** Resolute Bay and **(d)** Eureka (note the different scale for σ_Φ panels comparing to Cambridge Bay). Superposed in the scintillation panels is the H component of the ground magnetic field or riometer absorption measured at these stations. The H-component from Concordia station is shown in dotted line in panel **(d)**.

12:00 UT, both showed significantly smaller magnetic perturbation amplitudes (<200 nT) in the Southern Hemisphere. The vertical TEC, the rate of TEC change and σ_Φ scintillation index at Concordia (conjugate with Eureka) are also show in Fig. 7. The interhemispheric comparison in the central polar cap is discussed in Sect. 4.2.

Figure 8a–c shows percentage occurrence of phase scintillation σ_Φ exceeding 0.15 radians in the Canadian Arctic, Scandinavia and Antarctica from 5 to 7 April, mapped as a function of latitude and universal time (UT) on a grid 1° × 1 h, assuming the ionospheric pierce points (IPP) at 350 km altitude. The σ_Φ threshold is chosen to be sufficiently

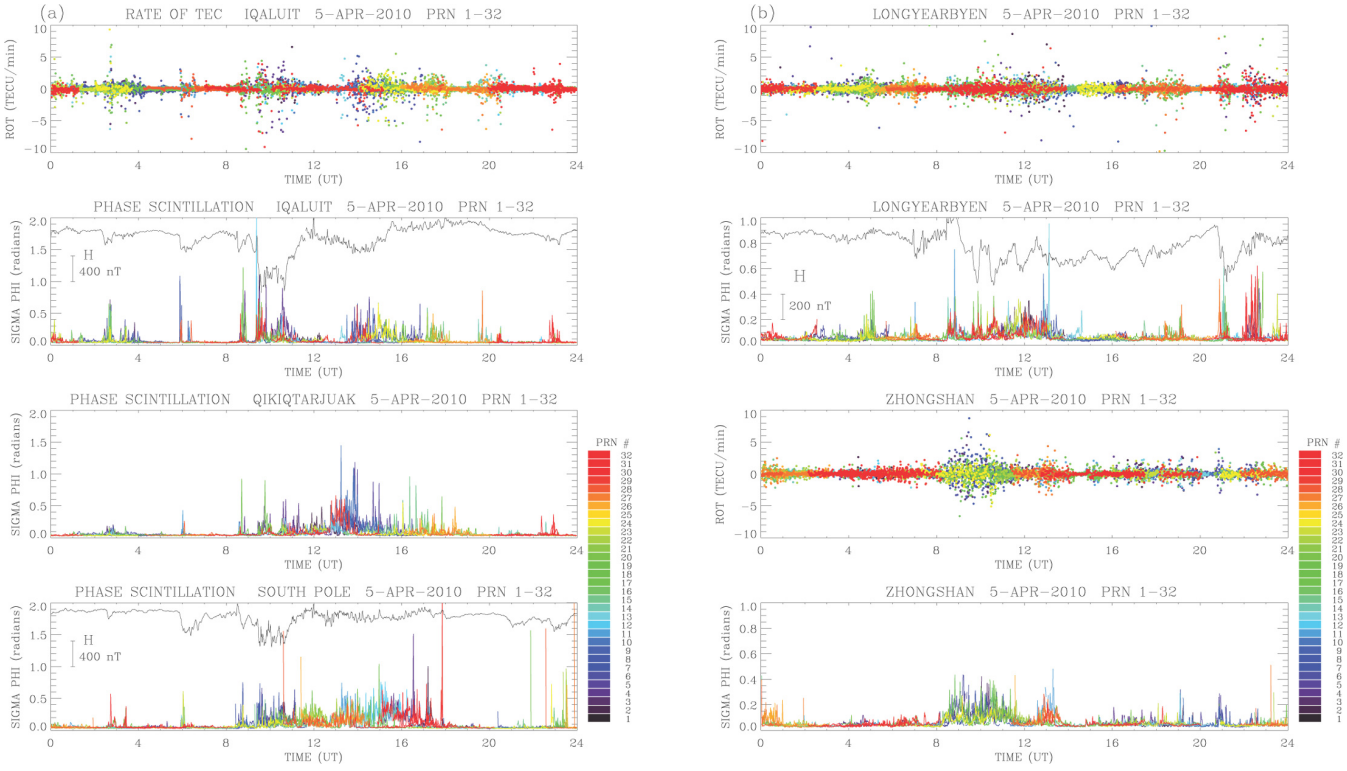

Fig. 6. The rate of TEC (ROT) change and phase scintillation index σ_Φ observed at elevations above 20° in **(a)** Iqaluit, Qikiqtarjuaq and South Pole and in **(b)** Longyearbyen and Zhongshan stations on 5 April 2010. Superposed in the scintillation panels for Iqaluit, South Pole and Longyearbyen is the H component of the ground magnetic field.

above the noise level for all receivers. Grey areas indicate either complete absence or insufficient number of data points to estimate statistically significant scintillation occurrence in a given grid cell (Spogli et al., 2009). The arrow indicates substorm onset that caused phase scintillation over a wide band of auroral latitudes in the CHAIN sector (Fig. 8a). After the substorm recovery a brief calm period centered about 12:00 UT coincided with a period of large northward IMF (Fig. 2). At about 12:30 UT, after a discontinuity in the IMF B_X and B_Y, and a reduction of the northward B_Z as the Earth entered the MC, ground magnetic perturbations and phase scintillation resumed at cusp/cleft latitudes from Cambridge Bay to Qikiqtarjuaq in the pre-noon sector (Fig. 8a). It should be noted that during this time the IMF B_Z was northward and then gradually rotated to become southward when the geomagnetic storm peaked on 6 April.

Figure 9a–f shows the scintillation occurrence as a function of magnetic latitude and magnetic local time (MLT) for CHAIN, Scandinavia and Antarctica on 5 and 6 April. The position of the statistical auroral oval for disturbed conditions (Feldstein and Starkov, 1967; Holzworth and Meng, 1975) is superposed. On the first day of the storm in the CHAIN sector, the scintillation occurrence was highest from 00:00 MLT at lower auroral latitudes to 12:00 MLT in the cusp (Fig. 9a). In Scandinavia (Fig. 9c), scintillation occurred mostly around magnetic noon when the high-speed solar wind arrived. In Antarctica (Fig. 9e), the highest scintillation occurrence was in the cusp in Zhongshan at the start of the storm and in the polar cap at all MLTs (Sect. 4.2). Unfortunately, there was a gap in the latitude coverage (∼68–70°) that prevented observing more auroral scintillation if present.

On 6 April, during the peak of the storm (Dst = −73 nT) when the IMF rotated southward as the geomagnetic activity intensified and the auroral oval expanded, the scintillation region shifted to lower auroral latitudes (Fig. 8a–b). As a function of MLT (Fig. 9b, d and f), the scintillation occurrence was highest in the auroral zone and low in the cusp. It was persistent in the southern polar cap but almost completely absent in the northern polar cap (see, Sect. 4.2). During the storm recovery on 7–8 April, episodic events of phase scintillation associated with auroral breakups as well as weak scintillation due to the cusp/cleft activity continued but gradually diminished (Fig. 8).

4.2 Polar cap activity

In the northern polar cap, only weak scintillation was observed in Resolute Bay and Eureka from 5 April to 7 April. It rarely exceeded the adopted σ_Φ threshold of 0.15 radians and therefore does not show in the scintillation occurrence

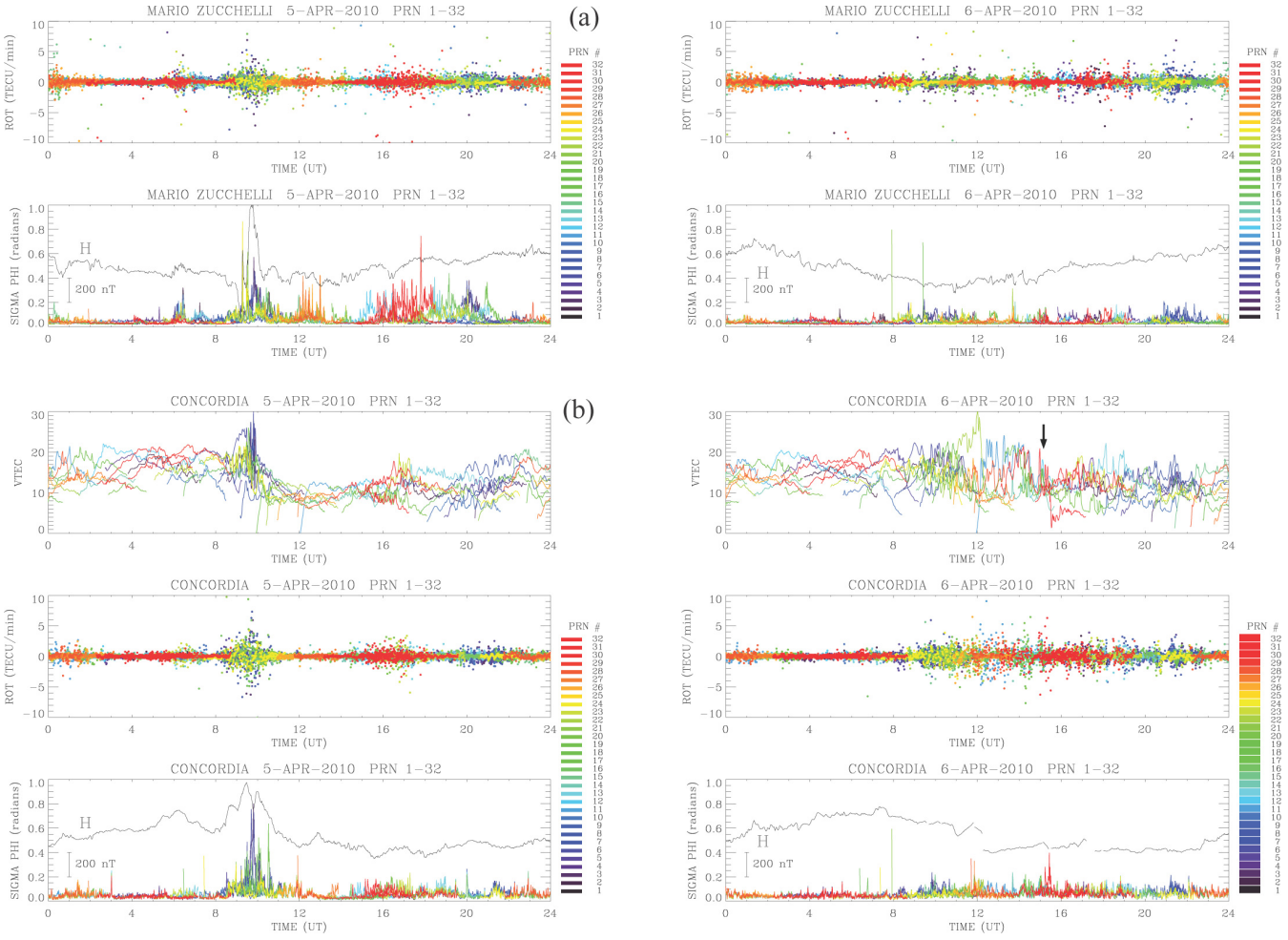

Fig. 7. The rate of TEC (ROT) change and phase scintillation index σ_Φ observed at elevations above 20° in **(a)** Mario Zucchelli (top two rows) and **(b)** Concordia stations (three bottom rows) on 5 and 6 April 2010. TEC values projected to the vertical are shown for Concordia with an arrow pointing to large variations due drifting patches before 16:00 UT on 6 April. Superposed in the scintillation panels is the H component of the ground magnetic field.

maps in Figs. 8a and 9a–b. Nevertheless, this relatively weak scintillation activity on 5 April was associated with moderate ground magnetic perturbations (Fig. 5c and d), which indicated dynamic ionospheric currents driven by coupling of solar wind ULF waves to the polar ionosphere for several hours. It should be noted that the orientation of the IMF was changing from predominantly southward before ~10:00 UT to predominantly northward later on. As a result, polar cap patches were formed before 10:00 UT while the strong northward IMF that followed was conducive of polar cap aurora. It is interesting to note how quickly the polar cap reacts to the IMF B_Z orientation. Patches were observed before 10:00 UT when the IMF B_Z was southward, and with the northward switch of B_Z precipitation into polar cap arcs was turned on (Fig. 10a).

On 5 April, patches were observed in both hemispheres although they were weaker, and scintillation occurrence was much lower, in the northern polar cap (Fig. 9). The ionosonde in Eureka experienced technical problem but observed weak polar patches before 09:00 UT. Figure 10a shows a fixed frequency ionogram for 2.7 MHz from Resolute Bay. A series of patches identified as U-shaped structures were observed mostly before 10:00 UT and the ionograms (Fig. 10b) indicated maximum *fo*F2 values up to 4 MHz. After the northward turning of the IMF, sporadic E-layer echoes appeared and the F-region patches weakened in the Northern Hemisphere. In the Southern Hemisphere, the F-region patches appeared to be denser although the maximum *fo*F2 value could not be determined with certainty because of oblique echoes. However, considering the angle-of-arrival information and limiting the echoes to within 10° off zenith it is estimated that *fo*F2 did not exceed 5 MHz. Later on, a strong sporadic E-layer was observed in both hemispheres. The sporadic E-layer ionization was produced

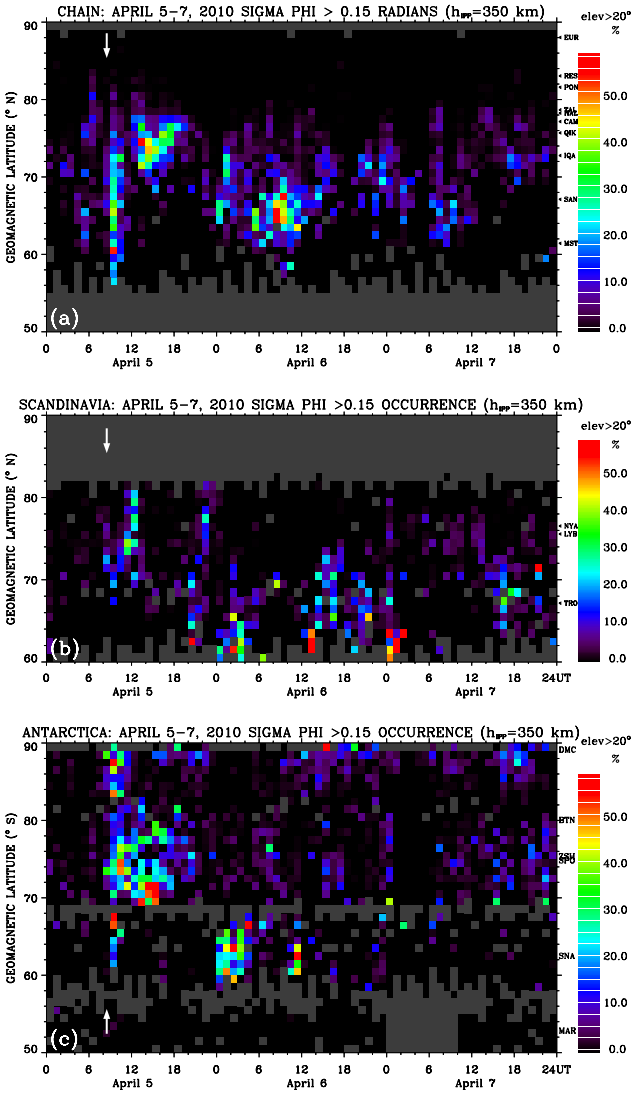

Fig. 8. Phase scintillation occurrence as a function of UT and CGM latitude for **(a)** CHAIN, **(b)** North European and **(c)** Antarctic arrays for 5–7 April 2010. The superposed white arrow indicates a substorm onset just after the arrival of the upstream shock.

by energetic particle precipitation that was observed by a DMSP-F17 satellite pass over northern Greenland west of Eureka at ∼11:55 UT, in daylight at this time. The DMSP particle detectors observed electron precipitation fluxes with energies of up to 4 keV in the polar cap (Fig. 11a) indicating presence of polar cap arcs (Newell et al., 2009). At 11:51 UT, the satellite was over Svalbard where the electron precipitation fluxes with energies of up to 3 keV were measured and phase scintillation was observed at Longyearbyen (Fig. 6b). Figure 9c shows that scintillation mostly occurred at latitudes near Svalbard in the noon to post-noon MLT sector. The ionization structure due to precipitation and associated cusp dynamics were the most likely causes of phase scintillation.

In contrast with the weak scintillation activity in the northern central polar cap in Resolute Bay and Eureka (Fig. 5c–d), the GPS receiver in Concordia observed relatively strong scintillation between 08:30 and 11:00 UT (Fig. 7b). The ground magnetic perturbations in Concordia and Eureka were similar in magnitude but were anti-correlated (Fig. 5d). The highest scintillation occurrence (Fig. 8c) was observed when the IMF B_Z oscillated between −15 and +10 nT and the IMF B_Y was predominantly negative (dawnward) but showing large oscillations. Dense F-region patches were observed by the ionosonde at Casey (Fig. 10c). These patches were formed in the cusp where the highest occurrence of phase scintillation was observed at Zhongshan (Figs. 8c and 9e). The patches then convected across the polar cap and caused scintillation in Concordia. The SuperDARN McMurdo radar observed patches (shown only for 6 April in Fig. 12) and strong convection (Fig. 4) in the polar cap until ∼09:30 UT when the IMF B_Z turned northward.

The phase scintillation in the southern polar cap over a wide range of MLTs was not only due to patches. As already discussed for the Northern Hemisphere, conditions of strong northward IMF on 5 April were favorable for polar cap auroras. From ∼11:00 UT the ionosonde at Casey observed a strong sporadic E-layer (Fig. 10c) suggesting energetic particle precipitation. Similarly to the DMSP-F17 satellite pass in the Northern Hemisphere, the DMSP-F16 pass over Concordia at 12:06 UT, in the nighttime ionosphere, detected polar cap electron precipitation with energies of up to 3 keV (Fig. 11b) indicating the presence of polar cap arcs at this time. Moderate scintillation in Concordia (Fig. 7b) continued into later UT hours when the MC magnetic field weakened but remained pointing northward (Fig. 2).

On 6 April, when the IMF in the MC rotated to point southward (Carlson Jr., 1994), patches were again observed by the ionosonde at Casey and a long series of F-region patches of decameter irregularities were observed with SuperDARN in the southern polar cap. Figure 12a and b shows backscatter power and LOS velocity for the Syowa East radar beam 0 and McMurdo radar beam 9 (the closest beams passing near the Concordia station). On 6 April, approaching or receding patches that can be identified as tilted bands of backscatter in Fig. 12a and b were observed by both radars. At times, the corresponding LOS velocities exceeded 1000 m s^{-1} either towards or away from the radars. This strong anti-sunward convection transported the patches over Concordia station where moderate phase scintillation and large TEC variations were observed for many hours after 09:00 UT (Figs. 7 and 8). Figure 12c shows a McMurdo radar scan of backscatter power at 15:09 UT showing two patches that produced large variations in TEC as they passed over Concordia (Fig. 7b). Superposed on the patches are IPPs for three PRNs near this time when phase scintillation index σ_Φ exceeded 0.2 radians that coincided with strong decameter irregularities. As a function of MLT, scintillation with σ_Φ exceeding 0.15 radians was observed for many hours in the

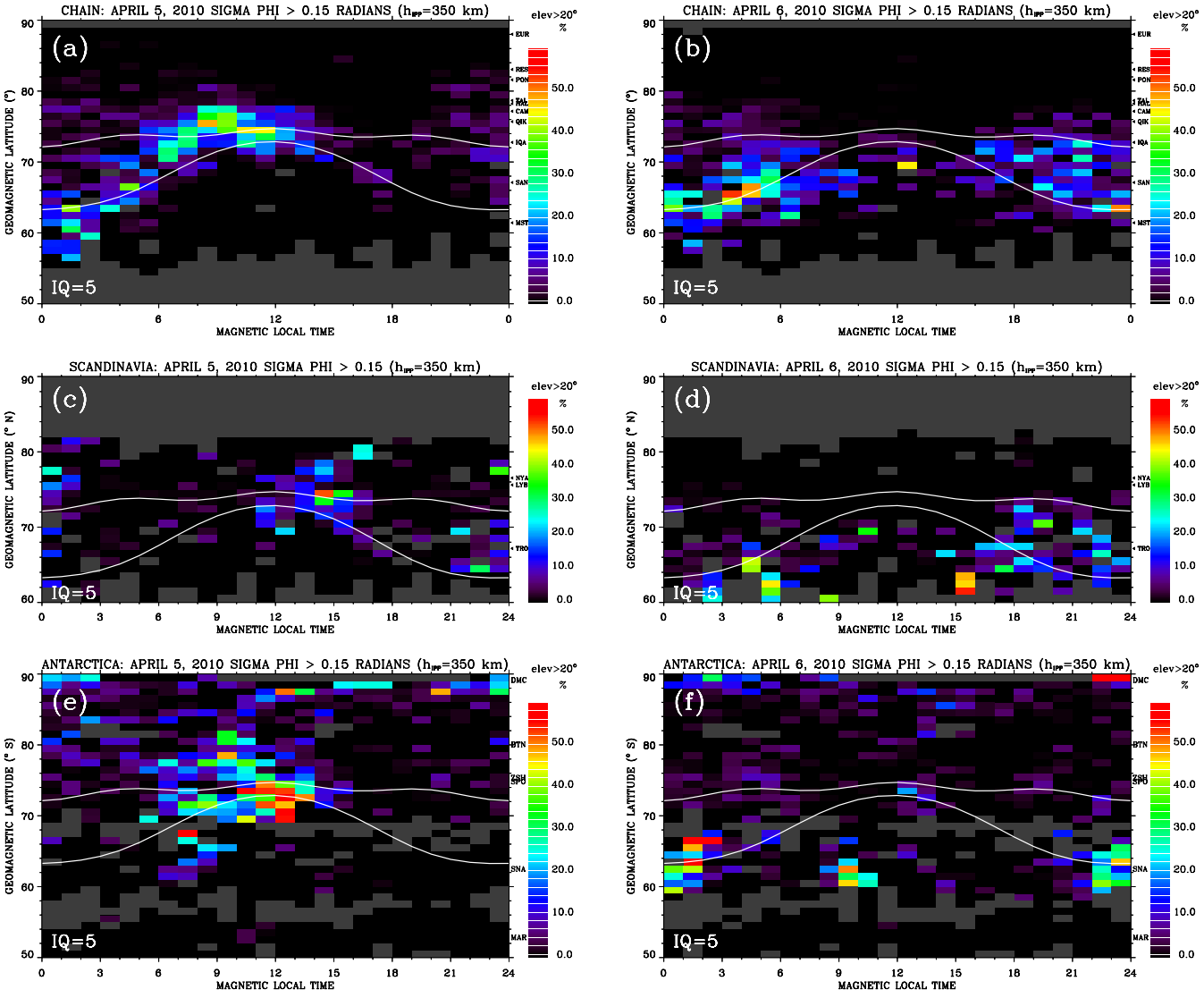

Fig. 9. Phase scintillation occurrence as a function of MLT and CGM latitude for **(a)–(b)** CHAIN, **(c)–(d)** North European and **(e)–(f)** Antarctic arrays for 5 and 6 April. Superposed in white line is the Feldstein statistical auroral oval for IQ = 5.

southern polar cap (Fig. 9f). In contrast, very low occurrence of radar backscatter and relatively weak patches were observed in the northern polar cap with SuperDARN and CADI ionosondes, respectively. Only weak scintillation (Fig. 5c–d) that is below the threshold of 0.15 radians in Fig. 9b was observed in Resolute Bay and Eureka.

5 Interhemispheric asymmetry in phase scintillation occurrence

At high latitudes, particularly in the cusp, the symmetry between expected conjugate ionospheric phenomena is often broken implying complicated magnetic field topology (Watanabe et al., 2007; Kabin, 2010). Similarities as well as asymmetries of conjugate auroras during auroral breakups and substorms have been observed (Sato et al., 1998, 2005; Laundal and Østgaard, 2009). The GPS phase scintillation at high latitudes during magnetic storms has been studied intensively in the past (Aarons et al., 2000; Basu et al., 2001). Studies of polar ionospheres during geomagnetic storms (e.g. Momani, 2008) revealed similarities and differences in GPS ionospheric scintillation, including asymmetrical occurrences of the ionospheric scintillation at conjugate points. Climatology studies in both hemispheres (Spogli et al., 2009; Li et al., 2010; Prikryl et al., 2011) showed that phase scintillation, as a function of magnetic local time and geomagnetic latitude, primarily occurs in the night-side auroral oval and ionospheric cusp, with scintillation regions shifting in latitude in response to varying geomagnetic activity. Phase scintillation and cycle slips were shown to be associated with

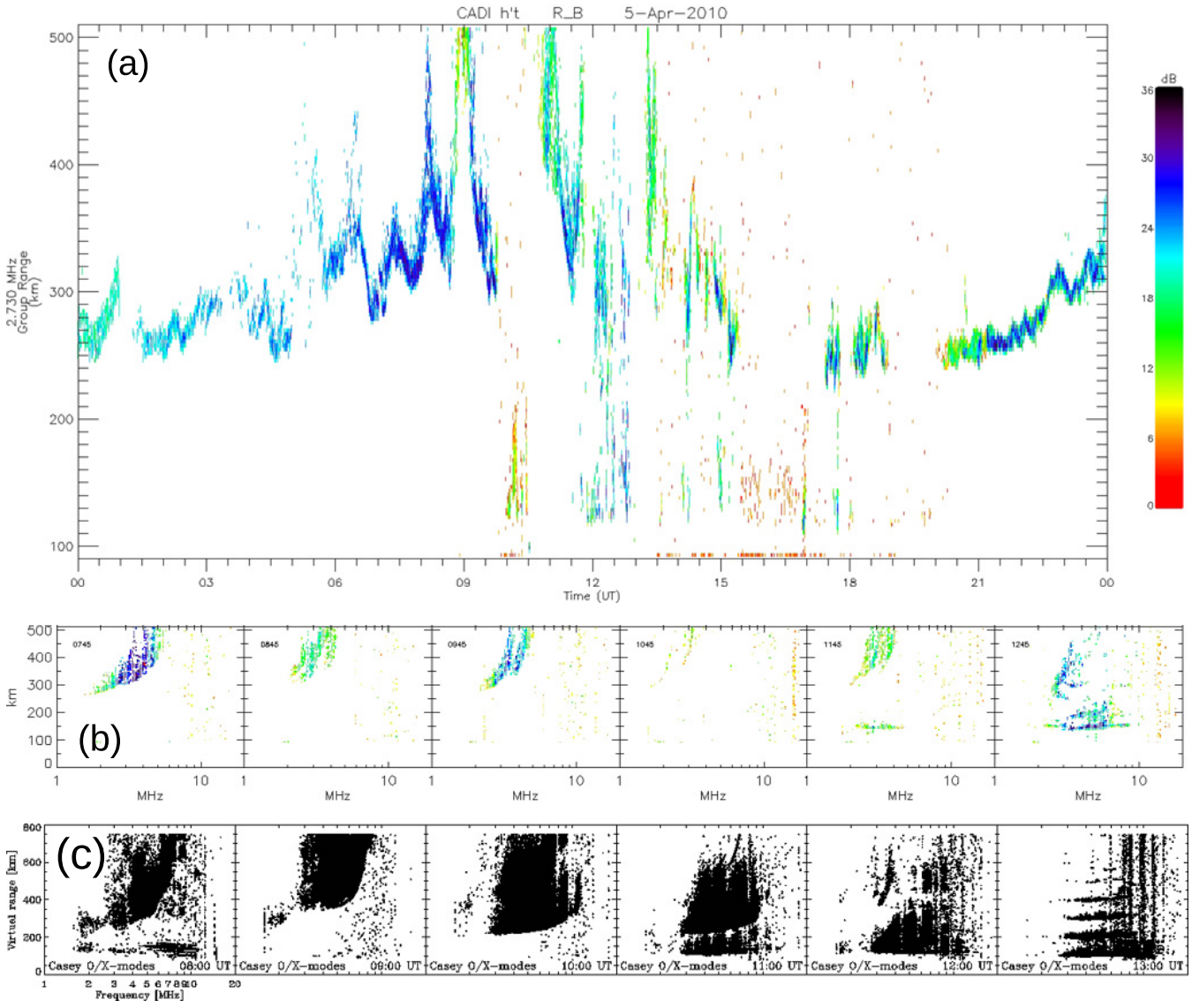

Fig. 10. (a) Fixed frequency and **(b)** swept frequency ionograms from Resolute Bay and **(c)** ionograms from Casey on 5 April 2010.

auroral arc brightenings and auroral substorms (Prikryl et al., 2010). In a statistical study based on one year of data acquired by a bipolar network, Alfonsi et al. (2011) obtained initial results describing the GPS scintillation occurrence in relation to the relative TEC variation and, in particular, the relationship between the irregularity scale size and the scintillation level. Li et al. (2010) conducted a statistical study of GPS phase scintillation occurrence at approximately conjugate locations at Ny-Alesund, Svalbard, and Larsemann Hills (Zhongshan station), Antarctica, which are typically located in the cusp and in the auroral oval or poleward of it in the night. They found maximum occurrence of scintillation during the local winter months. Their results also indicated that irregularities causing scintillation may be produced by precipitation into the cusp/cleft region. We have extended the interhemispheric comparison to other conjugate pairs, including South Pole and Qikiqtarjuaq.

The present multi-instrument study of the high-latitude ionospheres during an MC event further supports the above findings. We find that phase scintillation is associated with auroral and cusp events in both hemispheres. The phase scintillation occurrence and intensity that were observed in the auroral and cusp ionospheres over Cambridge Bay (Fig. 5a) were significantly higher than those at approximately conjugate Mario Zucchelli station (Figs. 7a and 8). Comparable concurrent scintillation was also observed at Qiqiktarjuaq and South Pole (Fig. 6a), and in Longyearbyen and Zhongshan (Fig. 6b).

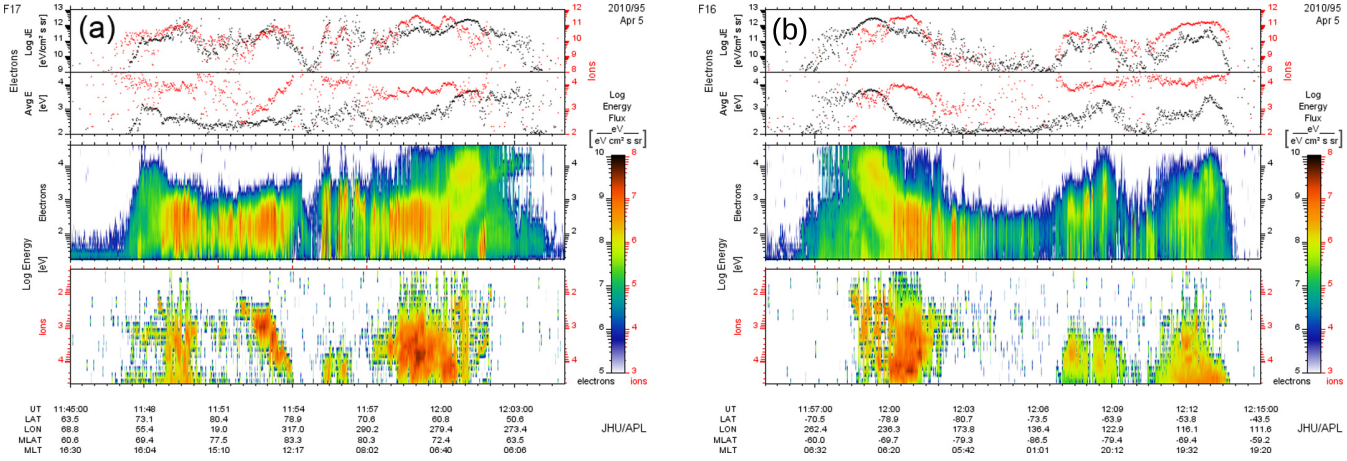

Fig. 11. Precipitating particle fluxes observed by DMSP satellites during passes over the **(a)** northern and **(b)** southern auroral ovals and polar caps. The F17 and F16 satellites passed nearest to Eureka and Concordia at ∼11:55 UT and 12:06 UT, respectively.

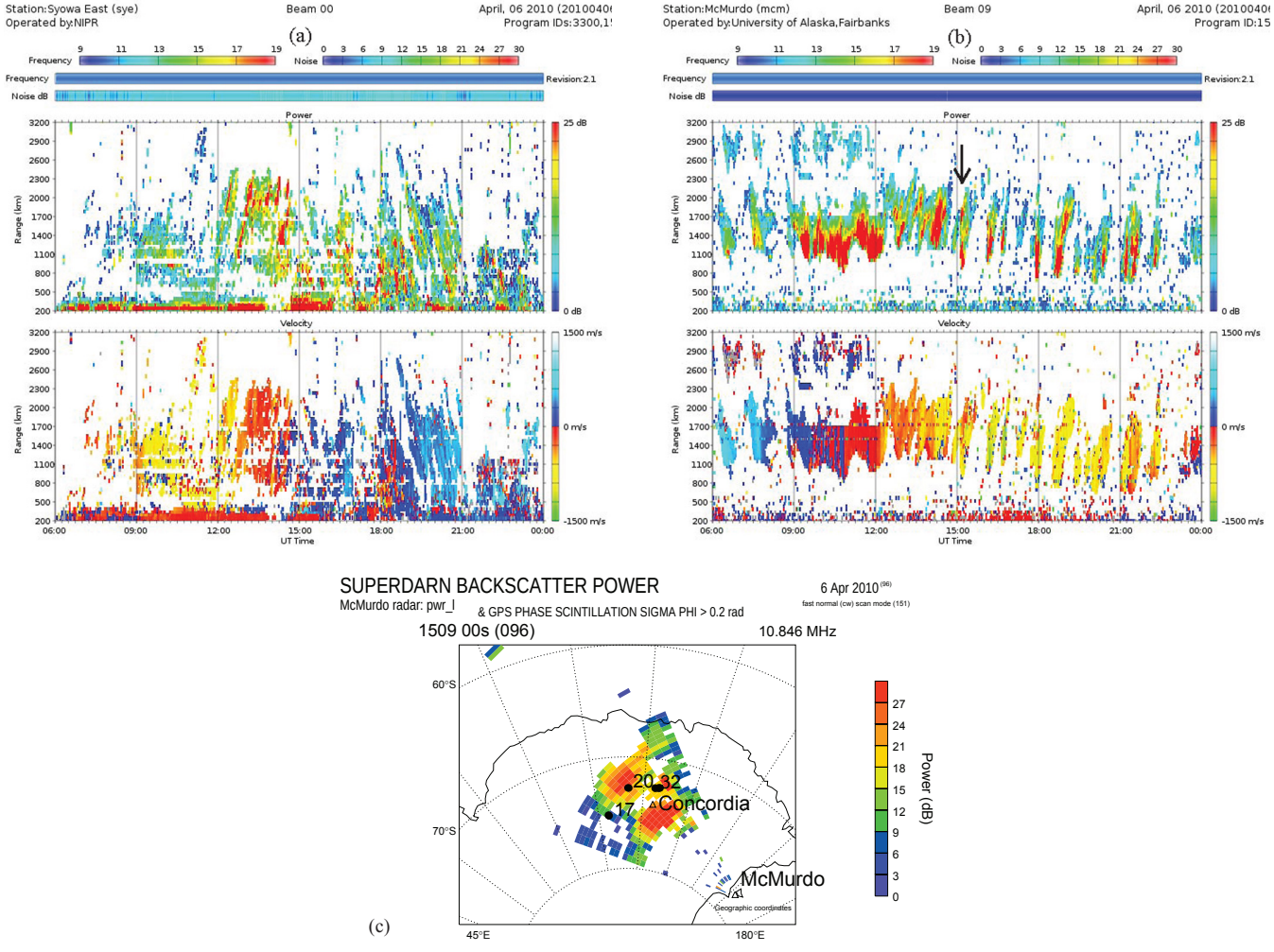

Fig. 12. The **(a)** Syowa East and **(b)** McMurdo radar backscatter power and LOS velocity showing a long series of polar cap patches. The arrow in panel **(b)** points to time 15:09 UT of **(c)** one scan showing McMurdo radar backscatter power and superposed GPS ionospheric pierce points at altitude 350 km when phase scintillation index σ_Φ exceeded 0.2 radians.

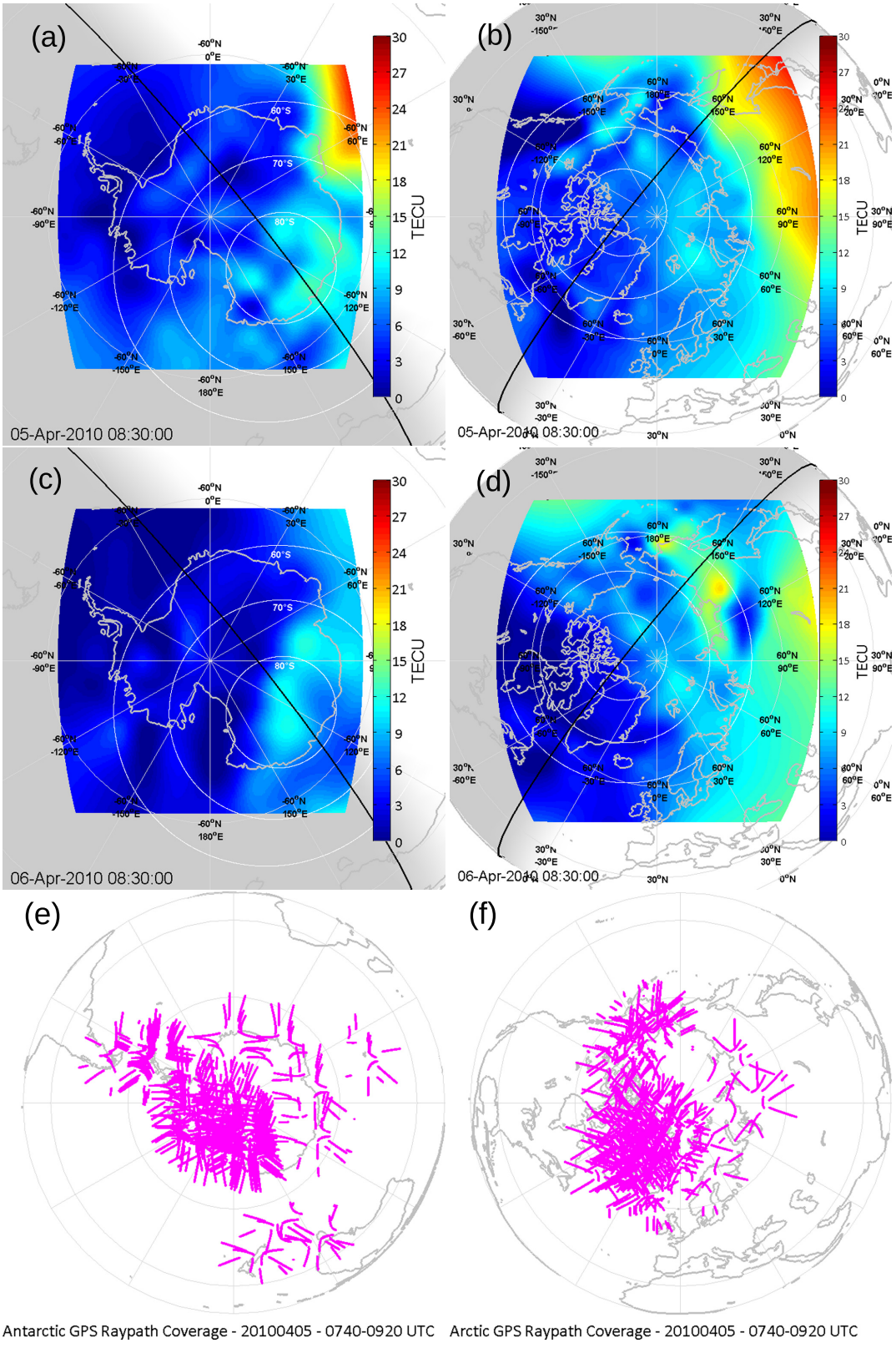

Fig. 13. **(a)**, **(c)** Southern and **(b)**, **(d)** Northern Hemisphere GPS vertical TEC maps reconstructed from 1 h data centered on 08:30 UT, 5 and 6 April 2010. Solar terminator (black line, ground level) and night-side shading is shown. Greenwich meridian longitude is the central vertical line in each image. Approximate geomagnetic latitude circles are centered on the 2005 AACGM pole. In Antarctica, TEC mapping used 50 sites from the PoleNet and IGS (International GNSS Service) (Kinrade et al., 2011). For the Arctic TEC maps, a total of 57 sites were used to reconstruct TEC maps. **(e)**, **(f)** The observed GPS ray path coverage was projected on to the ionosphere at an altitude of 350 km.

Interhemispheric asymmetry in TEC has already been briefly discussed in Sect. 1. In another study of the MC event of April 2010 (Kinrade et al., 2011) showed a case of a TEC enhancement over Antarctica on 5 April, between 10:00 and 19:00 UT (Kinrade et al., 2011; their Fig. 4). It extended towards South Pole station at the poleward edge of auroral oval where strong scintillation was observed. Only a weak to moderate scintillation was observed in Concordia at this time (Fig. 7b) when TEC in the central polar cap was very low. Although an earlier TEC map reconstructed for an hour centered at 08:30 UT (Fig. 13a) shows higher values of TEC in the polar cap, low density of ray paths in the polar cap region (Fig. 13e) diminishes our confidence in the TEC reconstruction result in the region that was sparsely populated with GPS receivers. Nevertheless, a moderate TEC enhancement on the dayside in the cusp would be consistent with the intense convection across solar terminator (Fig. 4b). At the same time, Northern Hemisphere TEC image suggests even lower TEC level just north of Scandinavia (Fig. 13b), where a strong antisunward convection occurred in the cusp (Fig. 4a). However, TEC was very low in the central polar cap over Greenland and the Canadian Arctic where the ray path coverage was good (Fig. 13f). Only weak patches (Fig. 10a) and scintillation (Fig. 5c–d) were observed at Eureka and Resolute Bay.

On 6 April, the TEC maps over Antarctica (Fig. 13c) showed a moderate TEC enhancement (>10 TECU above the lowest TEC in the nightside polar cap region adjacent to it) that appears to extend across the terminator into the polar cap over Concordia. Kinrade et al. (2011) presented a series of these TEC maps between 06:00 and 10:00 UT in their Fig. 5; all showing somewhat enhanced TEC on the dayside. Although such TEC values would not be considered unusual even on a quiet day as they occurred in the immediate vicinity of the cusp, the density of ray paths in the polar cap region was much lower than the density of ray paths over the geographic pole, which prevents us from drawing definitive conclusions. Nevertheless, a strong scintillation and TEC variations observed over Concordia (Fig. 7b) on 6 April were associated with abundant polar cap patches observed by SuperDARN radars (Fig. 12). At the same time, solar terminator in the Northern Hemisphere was located far from the cusp and moved poleward from it across the polar cap. TEC values remained low in the central polar cap over Eureka (Fig. 13d). No significant scintillation, F-region backscatter and only weak patches were observed in the northern polar cap. Thus we conclude that the difference in the location of solar terminator relative to the cusp can explain the observed interhemispheric asymmetry in the occurrence of polar cap patches and scintillation.

Interestingly, the asymmetry was particularly evident when the IMF rotated southward on 6 April (Fig. 8). There was no polar cap absorption event and riometers in Resolute Bay and Alert observed very low or no absorption. However, riometers in the northern auroral oval up to $\sim$78° N CGM latitude observed strong absorption, which must have strongly affected the HF propagation. Strong E-region backscatter was observed and a dense E-region could have reflected HF radio waves back to the ground causing multi-hop ground scatter, and this may have prevented HF propagation to F-region in the northern polar cap. Ionosonde F-region echoes in the northern polar cap were also generally weak or completely missing. This was in contrast with a denser F-region and strong HF backscatter in the southern polar cap.

The asymmetry between the northern and southern polar cap ionospheric structure is consistent with the seasonal variation in the occurrence of polar cap patches. Rodger and Graham (1996; their Fig. 2) found the highest occurrence of polar patches, as identified in HF-radar data from Halley, Antarctica, between equinox and winter (March to June) in 1989–1990, with a peak in April. They found minima in occurrence in midsummer and midwinter (January and July). In the Northern Hemisphere, the mean occurrence of HF backscatter attributed to polar patches from 2006–2008 averaged over 24 h (Prikryl et al., 2010; see their Fig. 9) is found highest from September to November, with a peak in November. The lowest HF backscatter occurrence in the northern polar cap is found from April to August. While the latter study was during solar minimum and statistics of patches by Rodger and Graham (1996) were for solar maximum, the seasonal variations in both hemispheres are very similar. Also, they are consistent with modeling and observations of plasma density structures in the central polar cap (Sojka et al., 1994; Basu et al., 1995).

Asymmetries in scintillation intensity and occurrence between the northern and southern polar caps are also found during a period of northward IMF. Comparable polar cap precipitation in both hemispheres was associated with stronger scintillation in the southern polar cap nighttime ionosphere, in contrast with sunlit E-region over Eureka and Resolute Bay. The higher-density sunlit ionosphere would increase conductivity thus shorting out the electric fields and inhibiting irregularity formation by smoothing out density gradients, which could have caused the asymmetry in scintillation strength.

In both hemispheres, the scintillation in the nightside auroral zone showed a significant shift to lower latitudes as the geomagnetic activity increased on 6 April. The auroral and cusp scintillation returned back to higher latitudes as the auroral oval contracted. Aarons et al. (1997) have shown that intense scintillation events are a function of the entry and exit of an observing site into the expanding auroral oval, the dynamics of the individual storm and the local magnetic time. This is also contained in the study by Ngwira et al. (2010). It is anticipated that in the future the scintillation receiver coverage in both hemispheres will improve to support further multi-instrument interhemispheric conjugate studies.

6 Summary and conclusions

Interhemispheric comparison of high-latitude ionospheric scintillation during a geomagnetic storm caused by a magnetic cloud embedded in high-speed solar wind is presented. Similarities but also asymmetries of the responses in the northern and southern auroral zones, cusps and polar caps are found. The arrival of the upstream shock, associated with a pressure pulse and southward IMF turning that caused a substorm onset, produced comparable phase scintillation occurrences at the poleward edge of the nightside auroral oval at approximately conjugate locations. An auroral breakup event that preceded the shock arrival and produced strong scintillation ($\sigma_\Phi > 1$ rad) and numerous cycle slips in the Northern Hemisphere resulted in weaker but coincident scintillation associated with small amplitude ground magnetic perturbation at southern stations. In the morning and in the cusp/cleft sector, comparable scintillation levels were observed in both hemispheres at about the same times.

Strong asymmetry was observed in the polar ionosphere when the upstream shock arrived and the IMF turned southward. Dense patches that were produced in the southern cusp and subsequently observed by an ionosonde at Casey caused strong scintillation at Concordia. However, only weak patches and scintillation were observed at Eureka and Resolute Bay. When the IMF turned strongly northward due to leading polarity of the bipolar magnetic cloud, comparable electron precipitation was observed by DMSP satellite passes over the sunlit northern and dark southern polar cap. Phase scintillation was moderate in the southern polar cap while only a weak scintillation was observed in the sunlit northern polar cap, probably due to reduced electron density gradients. After the IMF in the magnetic cloud rotated to southward for extended period of time and the geomagnetic storm intensified, no significant scintillation events or HF backscatter were detected in the northern polar cap. In contrast, moderate phase scintillation and variable TEC persisted for many hours at Concordia as a result of a long series of patches that traversed the southern polar cap. This asymmetry is explained by the difference in the location of solar terminator that was near the cusp in the Southern Hemisphere where sunlit ionospheric plasma observed in TEC maps was drawn into the central southern polar cap, while at the same time, solar terminator receded poleward from the northern cusp into the central northern polar cap. As a result, patch formation and scintillation was significantly reduced in the northern polar cap. This is consistent with the seasonal variation in occurrence of patches, which peaks in the southern polar cap while being at nearly lowest level in the northern polar cap in April.

Acknowledgements. Infrastructure funding for CHAIN was provided by the Canada Foundation for Innovation and the New Brunswick Innovation Foundation. CHAIN and CGSM operation is conducted in collaboration with the Canadian Space Agency (CSA). South Pole GPS operations are supported in part by NSF grants ANT-0840158 and ANT-0638587. These awards further support the University of Bath and Siena College GPS collaboration at South Pole and McMurdo Stations, Antarctica. GPS ground data from the PoleNet and IGS campaigns were obtained through the UNAVCO facility with support from the National Science Foundation (NSF) and National Aeronautics and Space Administration (NASA) under NSF Cooperative Agreement EAR-0735156. The funding for the operation of SuperDARN radars at Syowa Station in Antarctica was provided by the Research Program of Japanese Antarctic Research Expedition (JARE) of the Ministry of Education, Culture, Sports, Science, and Technology of Japan (MEXT). Operation of the McMurdo SuperDARN radar is supported by grant ANT-0944270 from the National Science Foundation Office of Polar Programs. The solar wind data were obtained from Goddard Space Flight Center Space Physics Data Facility OMNIWeb (http://omniweb.gsfc.nasa.gov/). The DMSP particle detectors were designed by Dave Hardy of Air Force Research Laboratory, and the data were obtained from Johns Hopkins University Applied Research Laboratory. The results presented in this paper rely on data collected at magnetic observatories operated by the Canadian GeoSpace Monitoring network, the Geological Survey of Canada, the Istituto Nazionale di Geofisica e Vulcanologia, the French Ecole et Observatoire des Sciences de la Terre (EOST), Strasbourg, and the South African National Space Agency. Management of the Concordia magnetic observatory is shared by Italian and French research institutes. The SANAE-IV observatory is managed by the South African National Antarctic Programme (SANAP). We thank the national institutes that support them and INTERMAGNET for promoting high standards of magnetic observatory practice. The authors thank for support by PNRA (Italian National Program for Antarctic Researches) and POLARNET-CNR.

Topical Editor K. Kauristie thanks two anonymous referees for their help in evaluating this paper.

References

Aarons, J., Mendillo, M., and Yantosea, R. T.: GPS Phase fluctuations in the equatorial region during sunspot minimum, Radio Sci. 32, 1535–1550, 1997.

Aarons, J., Lin, B., Mendillo, M., Liou, K., and Codrescu, M.: Global Positioning System phase fluctuations and ultraviolet images from the Polar satellite, J. Geophys. Res., 105, 5201–5213, doi:10.1029/1999JA900409, 2000.

Alfonsi, L., Spogli, L., De Franceschi, G., Romano, V., Aquino, M., Dodson, A., and Mitchell, C. N.: Bipolar climatology of GPS ionospheric scintillation at solar minimum, Radio Sci., 46, RS0D05, doi:10.1029/2010RS004571, 2011.

Basu, S., Basu, S., Sojka, J. J., Schunk, R. W., and MacKenzie, E.: Macroscale modeling and mesoscale observations of plasma density structures in the polar cap, Geophys. Res. Lett., 22, 881–884, doi:10.1029/95GL00467, 1995.

Basu, Su., Basu, S., Valladares, C. E., Yeh, H.-C., Su, S.-Y., MacKenzie, E., Sultan, P. J., Aarons, J., Rich, F. J., Doherty, P., Groves, K. M., and Bullet, T. W.: Ionospheric effects of major magnetic storms during the International Space Weather Period of September and October 1999: GPS observations, VHF/UHF scintillations, and in situ density structures at middle and equatorial latitudes, J. Geophys. Res., 106, 30389–30413, doi:10.1029/2001JA001116, 2001.

Burlaga, L., Sittler, E., Mariani, F., and Schwenn, R.: Magnetic loop behind an interplanetary shock – Voyager, Helios, and IMP 8 observations, J. Geophys. Res., 86, 6673–6684, 1981.

Bust, G. S., Garner, T. W., and Gaussiran II, T. L.: Ionospheric Data Assimilation Three Dimensional (IDA4D): A Global, Multi-Sensor, Electron Density Specification Algorithm, J. Geophys. Res., 109, A11312, doi:10.1029/2003JA010234, 2004.

Carlson Jr., H. C.: Dark polar ionosphere: Progress and future challenges, Radio Sci., 29, 157–165, 1994.

Chisham, G., Lester, M., Milan, S. E., Freeman, M. P., Bristow, W. A., Grocott, A., McWilliams, K. A., Ruohoniemi, J. M., Yeoman, T. K., Dyson, P. L., Greenwald, R. A., Kikuchi, T., Pinnock, M., Rash, J. P. S., Sato, N., Sofko, G. J., Villain J.-P., and Walker, A. D. M.: A decade of the Super Dual Auroral Radar Network (SuperDARN): Scientific achievements, new techniques and future directions, Surv. Geophys, 28, 33–109, doi:10.1007/s10712-007-9017-8, 2007.

De Franceschi, G., Alfonsi, L., and Romano, V.: Isacco: an Italian project to monitor the high latitude ionosphere by means of GPS receivers, GPS Solutions, 10, 263–267, doi:10.1007/s10291-006-0036-6, 2006.

De Franceschi. G., Alfonsi, L., Romano, V., Aquino, M., Dodson, A., Mitchell, C. N., Spencer P., and Wernik, A. W.: Dynamics of high-latitude patches and associated small-scale irregularities, J. Atmos. Solar-Terr. Phys., 70, 879–888, doi:10.1016/j.jastp.2007.05.018, 2008.

Donovan, E., Trondsen, T., Cogger, L., and Jackel, B.: Auroral imaging within the Canadian CANOPUS and NORSTAR projects, Sodankylä Geophysical Observatory Publications, 92, 109–112, 2003.

Echer, E., Alves, M. V., and Gonzalez, W. D.: A statistical study of magnetic cloud parameters and geoeffectiveness, J. Atmos. Solar-Terr. Phys., 67, 839–852, 2005.

Elsen, R. K., Winglee, R. M., Spann, J. F., Germany, G. A., Brittnacher, M., and Parks, G. K.: The auroral oval boundaries on January 10, 1997: A comparison of global magnetospheric simulations with UVI images, Geophys. Res. Lett., 25, 2585–2588, 1998.

Feldstein, Y. I. and Starkov, G. V.: Dynamics of auroral belt and polar geomagnetic disturbances, Planet. Space Sci., 15, 209–230, 1967.

Greenwald, R. A., Baker, K. B., Dudeney, J. R., Pinnock, M., Jones, T. B., Thomas, E. C., Villain, J.-P., Cerrisier, J.-C., Senior, C., Hanuise, C., Hunsucker, R. D., Sofko, G., Koehler, J., Nielsen, E., Pellinen, R., Walker, A.D.M., Sato, N., and Yamagishi, H.: DARN/ SUPERDARN A global view of the dynamics of high-latitude convection, Space Sci. Rev., 71, 761–796, 1995.

Ho, C. M., Mannucci, A. J., Lindqwister, U. J., Pi, X., Tsurutani, B. T., Sparks, L., Iijima, B. A., Wilson, B. D., Harris, I., and Reyes, M. J.: Global ionospheric TEC variations during January 10, 1997 storm, Geophys. Res. Lett., 25, 2589–2592, doi:10.1029/98GL00539, 1998.

Holzworth, R. H. and Meng, C.-I.: Mathematical Representation of the Auroral Oval, Geophys. Res. Lett., 2, 377–380, 1975.

Horvath, I. and Crozier, S.: Software developed for obtaining GPS derived total electron content values, Radio Sci., 42, RS2002, doi:10.1029/2006RS003452, 2007.

Huttunen, K. E. J., Schwenn, R., Bothmer, V., and Koskinen, H. E. J.: Properties and geoeffectiveness of magnetic clouds in the rising, maximum and early declining phases of solar cycle 23, Ann. Geophys., 23, 625–641, doi:10.5194/angeo-23-625-2005, 2005.

Jayachandran, P. T., Langley, R. B., MacDougall, J. W., Mushini, S. C., Pokhotelov, D., Hamza, A. M., Mann, I. R., Milling, D. K., Kale, Z. C., Chadwick, R., Kelly, T., Danskin, D. W., and Carrano, C. S.: Canadian High Arctic Ionospheric Network (CHAIN), Radio Sci., 44, RS0A03, doi:10.1029/2008RS004046, 2009.

Kabin, K.: Conjugacy between the two hemispheres at high latitudes in the null-separator model of the magnetosphere, American Geophysical Union, Fall Meeting Abstract #SM11A-1698, 2010.

Kinrade, J., Mitchell, C. N. , Yin, P., Smith, N., Bust, G. S., Jarvis, M. J., Maxfield, D. J., Rose, M. C., and Weatherwax, A. T.: Ionospheric scintillation over Antarctica during the storm of 5–6 April 2010, J. Geophys. Res., accepted, doi:10.1029/2011JA017073, 2011.

Kintner, P. M., Ledvina, B. M., and de Paula, E. R.: GPS and ionospheric scintillations, Space Weather, 5, S09003, doi:10.1029/2006SW000260, 2007.

Kumar, S. and Raizada, A.: Geoeffectiveness of magnetic clouds occurred during solar cycle 23, Planet. Space Sci., 58, 741–748, 2010.

Kumar, S., Chandra, H., and Sharma, S.: Geomagnetic storms and their ionospheric effects observed at the equatorial anomaly crest in the Indian Region, J. Atmos. Solar-Terr. Phys., 67, 581–594, 2005.

Laundal, K. M. and Østgaard, N.: Asymmetric auroral intensities in the Earth's Northern and Southern hemispheres, Nature, 460, 491–493, doi:10.1038/nature08154, 2009.

Li, G., Ning, B., Ren, Z., and Hu, L.: Statistics of GPS ionospheric scintillation and irregularities over polar regions at solar minimum GPS Solutions, 14, doi:10.1007/s10291-009-0156-x, 2010.

Liu, W. W.: Canadian space environment program and international living with a star, Adv. Space Res., 35, 51–60, 2005.

Mitchell, C. N., Alfonsi, Lu., De Franceschi, G., Lester, M., Romano, V., Wernik, A. W.: GPS TEC and scintillation measurements from the polar ionosphere during the October 2003 storm, Geophys. Res. Lett., 32, L12S03, doi:10.1029/2004GL021644, 2005.

Momani, M. A.: Investigation of the relationship between the storm enhanced density and ionospheric scintillation at conjugate points over the polar regions, J. Applied Sci., 8, 26–37, 2008.

Möstl, C., Temmer, M., Rollett, T., Farrugia, C. J., Liu, Y., Veronig, A. M., Leitner, M., Galvin, A. B., and Biernat, H. K.: STEREO and Wind observations of a fast ICME flank triggering a prolonged geomagnetic storm on 5–7 April 2010, Geophys. Res. Lett., 37, L24103, doi:10.1029/2010GL045175, 2010.

Newell, P. T., Liou, K., and Wilson, G. R.: Polar cap particle precipitation and aurora: Review and commentary , J. Atmos. Solar-Terr. Phys., 71, 199–215, 2009.

Ngwira, C. M., McKinnell, L.-A., and Cilliers, P., J.: GPS phase scintillation observed over a high-latitude Antarctic station during solar minimum, J. Atmos. Solar-Terr. Phys., 72, 718–725, 2010.

Osherovich, V. A., Fainberg, J., and Stone, R. G.: Solar wind quasi-invariant as a new index of solar activity, Geophys. Res. Lett., 26, 2597–2600, 1999.

Prikryl, P., Jayachandran, P. T., Mushini, S. C., Pokhotelov, D., MacDougall, J. W., Donovan, E., Spanswick, E., and St.-Maurice, J.-P.: GPS TEC, scintillation and cycle slips observed at high latitudes during solar minimum, Ann. Geophys., 28, 1307–1316, doi:10.5194/angeo-28-1307-2010, 2010.

Prikryl, P., Jayachandran, P. T., Mushini, S. C., and Chadwick, R.: Climatology of GPS phase scintillation and HF radar backscatter for the high-latitude ionosphere under solar minimum conditions, Ann. Geophys., 29, 377–392, doi:10.5194/angeo-29-377-2011, 2011.

Richardson, I. G. and Cane, H. V.: Geoeffectiveness (Dst and Kp) of interplanetary coronal mass ejections during 1995–2009 and implications for storm forecasting, Space Weather, 9, S07005, doi:10.1029/2011SW000670, 2011.

Richardson, I. G. and Zhang, J.: Multiple-step geomagnetic storms and their interplanetary drivers, Geophys. Res. Lett., 35, L06S07, doi:10.1029/2007GL032025, 2008.

Rodger, A. S. and Graham, A. C.: Diurnal and seasonal occurrence of polar patches, Ann. Geophys., 14, 533–537, doi:10.1007/s00585-996-0533-5, 1996.

Sato, N., Nagaoka, T., Hashimoto, K., and Saemundsson, T.: Conjugacy of isolated auroral arcs and nonconjugate auroral breakups, J. Geophys. Res., 103, 11641–11652, doi:10.1029/98JA00461, 1998.

Sato, N., Kadokura, A., Ebihara, Y., Deguchi, H., and Saemundsson, T.: Tracing geomagnetic conjugate points using exceptionally similar synchronous auroras, Geophys. Res. Lett., 32, L17109, doi:10.1029/2005GL023710, 2005.

Singer, H. J., Loto'Aniu, P. T., Green, J. C., Rodriguez, J. V., Anderson, B. J., Love, J. J., Angelopoulos, V., Baker, D. N., Connors, M. G., Denig, W. F., Donovan, E. F., Lecontel, O., Onsager, T. G., Nagatsuma, T., Runov, A., and Spanswick, E. L.: Multipoint observations of the large Substorm Associated with the Galaxy 15 Anomaly, Abstract SM22B-05, AGU Fall Meeting, 2010.

Sojka, J. J., Bowline, M. D., and Schunk, R. W.: Patches in the polar-cap ionosphere: UT and seasonal dependence, J. Geophys. Res., 99, 14959–14970, 1994.

Spencer, P. S. J. and Mitchell, C. N.: Imaging of fast moving electron-density structures in the polar cap, Ann. Geophys., 50, 427–434, 2007.

Spogli, L., Alfonsi, L., De Franceschi, G., Romano, V., Aquino, M. H. O., and Dodson, A.: Climatology of GPS ionospheric scintillations over high and mid-latitude European regions, Ann. Geophys., 27, 3429–3437, doi:10.5194/angeo-27-3429-2009, 2009.

Steele, D. P., McEwen, D. J., and Sivjee, G. G.: Ground-based optical observations from the north magnetic pole during the January 1997 magnetic cloud event, Geophys. Res. Lett., 25, 2573–2576, 1998.

Viljanen, A. and Häkkinen, L.: IMAGE magnetometer network, in: Satellite-ground based coordination sourcebook, edited by: Lockwood, M., Wild, M. N., and Opgenoorth, H. J., ESA publications SP-1198, 111–117, 1997.

Watanabe, M., Sofko, G. J., Kabin, K., Rankin, R., Ridley, A. J., Clauer, C. R., and Gombosi, T. I.: Origin of the interhemispheric potential mismatch of merging cells for interplanetary magnetic field B_Y-dominated periods, J. Geophys. Res., 112, A10205, doi:10.1029/2006JA012179, 2007.

Yermolaev, Y., Zastenker, G., Borodkova, N., Kovrazhkin, R., Nikolaeva, N., Nozdrachev, M., Saving, S., Skalsky, A., Zelenyi, L., and Nemecek, Z.: Statistic study of magnetosphere response to magnetic clouds: INTERBALL multi-satellite observations: Physics and Chemistry of the Earth, Part C: Solar, Terr. Planet. Sci., 25, 177–180, 2000.